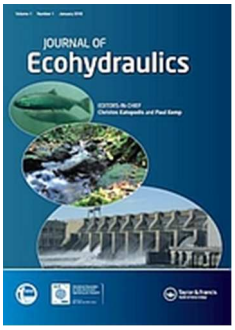

POSITION CHOICE AND SWIMMING COSTS OF JUVENILE ATLANTIC SALMON SALMO SALAR IN TURBULENT FLOW

Journal:	*Journal of Ecohydraulics*
Manuscript ID	Draft
Manuscript Type:	Original Article
Date Submitted by the Author:	n/a
Complete List of Authors:	Wilkes, Martin; Coventry University, Centre for Agroecology, Water and Resilience; University of Worcester Enders, Eva; Fisheries and Oceans Canada Central and Arctic Region, Freshwater Institute Silva, Ana; Norsk Institutt for Naturforskning Acreman, Michael; Centre for Ecology and Hydrology Maddock, Ian; University of Worcester
Keywords:	Swimming costs, bioenergetics, turbulence, hydrodynamics, habitat, Atlantic salmon
Abstract:	Swimming costs (SC) for fish have been shown to be affected by turbulence. However, this idea has not yet been implemented in habitat models, which often represent hydraulics using water velocity averaged over time and space. In this study, we analysed the habitat selection of individual juvenile Atlantic salmon Salmo salar (L. 1758) in relation to predicted SC in the turbulent flow of a large outdoor flume. We used a previously published SC model parameterised using mean velocity, turbulence intensity, water temperature and fish mass. Results showed that 86% of fish chose locations with significantly lower predicted SC than expected at random ($p<0.05$). Position choice was negatively related to predicted SC, mean velocity, spatial velocity gradient, and Reynolds stresses. Based on the findings, a novel habitat suitability curve is recommended for juvenile Atlantic salmon. The results are expected to contribute towards the improvement of bioenergetics modelling to increase our understanding of the impacts of environmental changes and management activities.

POSITION CHOICE AND SWIMMING COSTS OF JUVENILE ATLANTIC SALMON *SALMO SALAR* IN TURBULENT FLOW

Wilkes MA[1,2*], Enders EC[3], Silva AT[4], Acreman M[5], Maddock I[2]

[1]Centre for Agroecology, Water & Resilience, Coventry University, Coventry, United Kingdom

[2]Institute of Science and the Environment, University of Worcester, Worcester, United Kindom

[3]Fisheries and Oceans Canada, Winnipeg, Canada

[4]Norwegian Institute for Nature Research, Trondheim, Norway

[5]Centre for Ecology & Hydrology, Wallingford, United Kingdom

*Corresponding author: Centre for Agroecology, Water & Resilience, Coventry University, Coventry, CV1 5FB, United Kingdom; martin.wilkes@coventry.ac.uk; +44 7557 425307

POSITION CHOICE AND SWIMMING COSTS OF JUVENILE ATLANTIC SALMON *SALMO SALAR* IN TURBULENT FLOW

Abstract

Swimming costs (SC) for fish have been shown to be affected by turbulence. However, this idea has not yet been implemented in habitat models, which often represent hydraulics using water velocity averaged over time and space. In this study, we analysed the habitat selection of individual juvenile Atlantic salmon *Salmo salar* (L. 1758) in relation to predicted SC in the turbulent flow of a large outdoor flume. We used a previously published SC model parameterised using mean velocity, turbulence intensity, water temperature and fish mass. Results showed that 86% of fish chose locations with significantly lower predicted SC than expected at random ($p<0.05$). Position choice was negatively related to predicted SC, mean velocity, spatial velocity gradient, and Reynolds stresses. Based on the findings, a novel habitat suitability curve is recommended for juvenile Atlantic salmon. The results are expected to contribute towards the improvement of bioenergetics modelling to increase our understanding of the impacts of environmental changes and management activities.

Keywords: Swimming costs; bioenergetics; turbulence; hydrodynamics; habitat; Atlantic salmon.

POSITION CHOICE AND SWIMMING COSTS OF JUVENILE ATLANTIC SALMON *SALMO SALAR* IN TURBULENT FLOW

Introduction

In recent decades two parallel trends in river research and management have led to an increasing focus on the hydrodynamics of river ecosystems (Nikora 2010; Wilkes et al. 2013) and a proliferation in the development of bioenergetics models for fish (Fausch 2014; Jørgensen et al. 2016), which include an important foraging component (*e.g.* Hughes & Dill 1990; Hill & Grossman 1993; Booker et al. 2004). Such forage-based models seek to predict the distribution, growth, abundance or biomass of drift feeding fish by modelling the fish's net energetic intake (NEI) as a function of the gross energetic intake (GEI) acquired through prey capture and the associated swimming costs (SC):

$$NEI = GEI - SC \quad (1)$$

(Piccolo et al. 2014). Their appeal over traditional hydraulic habitat models, such as PHABSIM (Physical Habitat Simulation system; Milhous et al. 1984), is that they have mechanistic foundations (Lancaster & Downes 2010; Meineri et al. 2014). Traditional hydraulic habitat models rely on correlative habitat suitability curves derived from measuring simple descriptions of the fluvial environment - water velocity, water depth, and substrate where fish are present and absent - resulting in an index of habitat suitability. On the other hand, forage-based models incorporate the costs and benefits of food acquisition in an ecologically realistic way (Hayes et al., 2016).

In traditional hydraulic habitat models water velocity is represented by mean column velocity, whereas the SC component (equation 1) of forage-based models is typically estimated with the assumption of sustained swimming at constant speeds (Piccolo et al.

2014), although corrections for accelerations and turns may be made (Hayes et al., 2016). The use of mean column velocity or constant swimming speeds, however, provides a far from complete description given that fish are swimming in spatiotemporally dynamic, three-dimensional turbulent flow. Laboratory studies have revealed strong relationships between turbulent flow and SC, calling for turbulence to be considered in habitat models (Enders & Boisclair 2016). Respirometer studies by Enders et al. (2003) demonstrated that juvenile Atlantic salmon *Salmo salar* (L. 1758) may consume significantly more energy when swimming in unpredictable turbulent flow. An existing model for predicting SC based on steady swimming at mean velocity (Boisclair & Tang 1993) did not match the data of Enders et al. (2003) well, leading to the development of a new turbulent SC model (Enders et al. 2005). Turbulence in this case was described as the standard deviation of the primary velocity component (u_{SD}) but several other studies suggest that the energy efficiency of fish locomotion may be dependent on other hydrodynamic properties. In particular, the direction relative to fish body shape, the scale relative to fish body length, and the periodicity of the turbulent flow may all be important (Webb 2004; Liao 2007, Lacey et al. 2012).

Previous laboratory work with laterally compressed fish has shown that eddies rotating on a horizontal axis may, depending on the ratio of eddy size to fish body length, destabilize fish and result in increased energetic costs (Pavlov et al. 2000; Lupandin 2005; Tritico & Cotel 2010). Silva et al. (2011 2012) found that Iberian barbel *Luciobarbus bocagei* (L. 1758) avoided areas of high Reynolds shear stress, which describes transport occurring through displacements of fluid particles without a change in momentum (accelerations and decelerations of fluid particles due to pressure and viscous forces). The mechanism appeared to be postural challenges leading to increased energetic costs at high Reynolds stresses. On the other hand, relatively predictable (highly periodic), vertically oriented eddies associated with cylinder wakes allowed rainbow trout *Onchorynchus mykiss* (Walbaum 1792) to reduce

SC by Kármán gaiting (Liao et al. 2003; Taguchi & Liao 2011). Further reductions in SC have been observed in rainbow trout entraining on obstacles (Cook & Coughlin 2010; Przybilla et al. 2010; Taguchi & Liao 2011). Spatial gradients in velocity have also been implicated in the position choice of juvenile Atlantic salmon and brown trout *S. trutta* (L. 1758) due to their distinctive 'sit-and-wait' feeding behaviour (Hayes & Jowett 1994; Booker et al. 2004).

This study aimed to advance knowledge of how turbulence affects habitat selection in juvenile Atlantic salmon by: (i) testing the ability of a turbulent SC model (Enders et al. 2005) to predict position choices in wild fish; and (ii) assessing whether this prediction may be improved upon by taking into consideration other properties of the turbulent flow, including intensity, periodicity, direction, and scale. It was hypothesised that fish would occupy positions within an artificial habitat associated with energetically favourable hydrodynamic conditions that are likely to minimise SC.

Material and methods

Experimental Setup

Experiments were conducted in a 2 m long section of an outdoor flume at the International Centre for Ecohydraulics Research (ICER), University of Southampton. The flume is 2 m wide and 60 m long with a trapezoidal cross-section and a concrete bed. The test section was covered with a heavy canvass tent. Test conditions were created using artificial habitat features consisting of 24 small (50 mm in diameter) and 16 large (100 mm in diameter) transparent plastic hemispheres that were fixed to the bottom of the stream channel (Figure 1). Transparent habitat features were used to reduce the likelihood of fish responding to visual cues. We further reduced this likelihood by performing trials in darkness (<0.001 lux).

Discharge (0.056 $m^3 s^{-1}$) and flow depth (16.5 cm) were constant throughout the experiments. The flow depth was set to be within the natural range of depths reported to be used by juvenile Atlantic salmon (Symons and Heland 1978; Kennedy and Strange 1982; Morantz et al. 1987; Heggenes 1990). During the experiments, water temperature was maintained at 15 °C (± 0.1 °C). Instantaneous water velocities at set locations around the hemispheres (Figure 1) were measured with a 3-D acoustic Doppler velocimeter (ADV) (model Vectrino II, Nortek International, Rud, Norway) at a frequency of 25 Hz for 90 s, providing a highly resolved characterisation of the turbulent flow. This frequency and record length has been shown to be optimal in gravel-bed rivers (Buffin-Bélanger and Roy 2005). Velocities were measured at 20-24 mm above the bottom of the flume, to approximate the focal point velocity of juvenile salmonids (Heggenes & Saltveit 1990; Riehle & Griffith 1993).

[Figure 1 near here]

Experimental procedure

A total of 46 juvenile (0+) Atlantic salmon (96.30 ± 0.51 mm TL) were electrofished (50 Hz pulsed DC) from the River Frome, Dorset, UK on 6 September 2012 and transported (tanks with aerated river water at a temperature of 12 °C) to the ICER experimental facility. Fish were maintained in a holding tank (1000 L; filtered, oxygenated, dechlorinated mains water) and acclimated for a minimum of 7 d to ambient temperatures (14.6 ± 1.4 °C) and natural photoperiod before the trials began. Efficient aeration and filtration systems were used and water quality was monitored and maintained within the range considered suitable for fish husbandry. Water was regularly replenished. During this time, fish were fed with defrosted chironomid larvae but not fed for 24 h prior to experimental trials. Each trial began by adding an individual fish to the flume at a random position in the test section. After 30 min to acclimatise to the flow and explore the habitat, the position of each fish was recorded for 10

min using an infra-red camera (Sony 1000TVL, 720P, IR-CUT). All trials were conducted at night to avoid any confounding diurnal effects. Fish were not fed during the trials. At the end of each trial, the fish was removed from the test section and held separately from other fish for 24 h to monitor its health. Trials were conducted between dusk and dawn on 13, 14 and 15 September 2012.

Data processing

ADV data were post-processed using a phase-space filter (>95% good pass criterion), with inconsistent data points replaced using a third-order polynomial fitted to the data either side of the spike (Parsheh et al. 2010). The data were rotated into the resultant vector in three dimensions, so that:

$$\bar{v} = \bar{w} = 0 \quad (2)$$

where *v'*, and *w'* are instantaneous velocities in the vertical and spanwise directions respectively, and overbars denote ensemble averages. The rotated data were used to calculate the following hydraulic variables: mean velocity (U), turbulence intensity (u_{SD}) and Reynolds stresses on the streamwise-vertical (τ_{uv}), and streamwise-lateral (τ_{uw}) planes:

$$\tau_{uv} = \rho\overline{uv}\,,\ \tau_{uw} = \rho\overline{uw} \quad (3)$$

where ρ is the water density (1000 kg m^{-3}) and *u'* is the instantaneous velocity in the streamwise component.

Average eddy length (L_u) was calculated using a second-order autoregressive model:

$$L_u = u_t U \quad (4)$$

$$u_t = a_1 u_{t-1} + a_2 u_{t-2} + e_t$$

where a_1 and a_2 are coefficients of the velocity at a given time lag and e_t is a random component (Clifford and French 1993a). All the hydraulic variables were interpolated to a 25 mm mesh grid using an Ordinary Kriging method (Oliver 1990) in ArcGIS 10 (ESRI 2011). The 25 mm mesh size was chosen as a scale consistent with the fish size, the scale of the hemispheres and the resolution of the ADV measurements.

SC was predicted for each cell according to the equation for the turbulent SC model (SC_{pred}) (Enders et al. 2005):

$$logSC_{pred} = 0.23logT + 0.64logM + 2.43logU + 0.67logu_{SD} - 4.06 \quad (5)$$

where T is water temperature and M is the fish body mass. SC_{pred} was calculated for the average mass of fish used in this study (9 g) at a temperature of 15 °C. Spatial velocity gradient (V_{grad}) was also calculated for each cell as the standard deviation of U in all neighbouring cells within a 200 mm radius (approximately two body lengths, the foraging radius of juvenile salmonids; Fausch 1984).

Fish focal position was recorded manually using tracking software (Kinovea 0.8.15) every 5 s, giving 121 observations per fish referenced to the same grid cell system as the hydraulic data. These results were used to calculate a selection index (SI) of the fish for each cell. This index was calculated based on the number of times a fish was observed in that cell (cell occupancy, CO_{cell}):

(6)

$$CO_{cell} = \sum_{i=1}^{n} fish_{i,cell}$$

$$SI = \frac{CO_{cell}}{CO_{max}}$$

where $fish_{i,cell}$ is the occupancy count for each fish in each cell and CO_{max} is the maximum cell occupancy or, in other words, the CO_{cell} associated with the most popular cell.

Statistical analyses

A permutation test was used to test the null hypothesis that fish chose cells at random, independently of SC_{pred}. The null distributions of SC_{pred} were constructed from 10,000 bootstrap samples of 121 random cells (with replacement). For each fish, the probability (p) that the fish chose cells at random was calculated as:

(7)

$$p = \frac{\sum_{i=1}^{n}(SC_{null} \geq SC_{fish}}{k} - 1$$

where k=10,000 permutations, SC_{null} is the mean SC_{pred} associated with each bootstrap sample and SC_{fish} is the mean SC_{pred} of cells used by each fish.

Generalised linear models were used to predict SI using two sets of explanatory variables: (i) SC_{pred}; and (ii) a linear combination of hydrodynamic variables (U, u_{SD}, τ_{uv}, τ_{uw}, L_u, and V_{grad} were considered), which we term the 'hydrodynamic habitat model'. Habitat selection was found to follow a Poisson distribution. Nevertheless, due to the high number of zeros as result of the fact that fish could not occupy all cells (even where the habitat was suitable), a zero-inflated negative binomial (ZINB) model was applied in order to deal with overdispersion:

$$g(\mu_i) = \beta_0 + X^T\beta, \;\; g(\pi_i) = \beta_0 + X^T\beta \quad (8)$$

where g is a link function, β_0 is the intercept, X^T is a vector of m predictor variables, and β is a vector of m regression coefficients. Thus, we modelled the probability of finding false zeros (*i.e.*, locations in which fish were not observed but nevertheless represented suitable habitat; see Zuur et al. 2009) separately to the count (SI) data. A log link was used for the count model (μ), whilst the binomial model (π) was facilitated by a logit link function.

The Akaike information criterion (AIC), an inverse measure of goodness-of-fit, was used to compare results for the SC_{pred} and hydrodynamic habitat models. AIC was also used for model selection along with likelihood ratio tests for nested models. All statistical procedures were carried out using R3.2.4 (R Core Team 2015).

Results

Flow conditions in the test section

Resultant mean velocities and turbulence intensities ranged from 0.16 to 20 cm s^{-1} and 0.38 to 8.13 cm s^{-1}, respectively (Figure 2a-b). A wide range of length scales ($0.26<L_u<34.98$ cm) were distributed throughout the test arena (Figure 2c). Regions of highest turbulence intensity (Figure 2b), Reynolds shear stresses (Figure 2d-e), and flow divergence and convergence (Figure 2f) were associated with bed protrusions, conditions typically associated with flow around pebble clusters (Buffin-Bélanger and Roy 1998; Lawless & Robert 2001). Velocity spectra showed peaks in the region 0.01-0.2 Hz and typically became flattened downstream of hemispheres (Figure 3). The conditions on each side of the test section were noticeably different, with the right side generally exhibiting higher velocities, greater turbulence intensities, and larger scales. SC_{pred} was distributed between 0.01 and 3.89 mg O_2 h^{-1} (0.19-75.39 J h^{-1} assuming no anaerobic component; Heath, 1995). Following the general hydraulic

patterns observed, SC_{pred} was higher on the right side of the test section and in the vicinity of bed obstacles (Figure 4).

[Figure 2 near here]

[Figure 3 near here]

[Figure 4 near here]

Habitat selection

Fish moved around the test section to varying degrees. Some fish remained in the same or adjoining cells for the duration of observations, whereas others used a wider range of SC_{pred}. Figure 5a shows two fish trajectories that exemplify this range of behaviours. Thus, individual fish were classified as 'station-holding' (remaining in the same or adjoining cells for the duration of observations) or 'searching' (Table 1). Fish most often selected cells close to hemispheres (both large and small hemispheres) and the edges of the test section (Figure 5b). Figure 6 shows the frequency distribution of mean SC_{pred} under the null model (random cell selection). The permutation tests revealed that 86% of fish chose cells with significantly lower mean SC_{pred} than expected at random ($p<0.05$), including all fish that exhibited station-holding behaviour for the duration of observations (Table 1). Results of ZINB modelling showed that SC_{pred} was negatively related to habitat selection (Figure 7). Observed *SI* was clustered around low SC_{pred}. The probability of finding a false zero (*i.e.* where the habitat is suitable but no fish were observed) was consistently low (Figure 7). Count (*SI*) model coefficients were highly significant (Table 2).

[Table 1 near here]

[Table 2 near here]

[Figure 5 near here]

[Figure 6 near here]

[Figure 7 near here]

Hydrodynamic habitat model

Due to intercorrelation between U, u_{SD} and L_u, ($0.78<r<0.95$), only U, τ_{uv}, τ_{uw} and V_{grad} were entered as explanatory variables for the hydrodynamic habitat model. In the case of τ_{uw}, the magnitude of turbulence-related disturbances on this horizontal plane, rather than the direction, is of most interest. Thus, absolute values were used ($|\tau_{uw}|$).

Reynolds stresses were the weakest contributing variables to the model and, therefore, we examined the effect of dropping both of these variables simultaneously. The solution that dropped both τ_{uv} and $|\tau_{uw}|$ from the count model was optimum as this was the most parsimonious model with the lowest AIC (Table 3). All coefficients for both the count and binomial components of this optimum model were significant (Table 4). Predicted *SI* was negatively related to U and V_{grad}, whilst the probability of finding false zeros, where the habitat was suitable but no fish were observed, was also negatively related to Reynolds stresses (Figure 8). The AIC of the hydrodynamic habitat model was lower than for the SC_{pred} model ($6925.55<6967.16$).

[Table 3 near here]

[Table 4 near here]

[Figure 8 near here]

Discussion

This study advances understanding of the role of swimming energetics and turbulent flow in the habitat selection of juvenile Atlantic salmon in a realistic hydrodynamic environment. Mean velocities and turbulence intensities were within the range used to construct the SC model of Enders et al. (2005). Furthermore, all hydrodynamic variables were within an order of magnitude of those reported in gravel-bed rivers (Lacey et al. 2007; Smith & Brannon 2007; Roy et al. 2010). Our findings suggest that turbulence and swimming energetics do affect position choice. The results of permutation tests and ZINB modelling using a turbulent SC model (Enders et al. 2005) supported the hypothesis that the fish would select locations that minimised SC.

A hydrodynamic habitat model that included U, V_{grad}, and Reynolds stresses performed better than the SC_{pred} model, as evidenced by a lower AIC despite the model being less parsimonious. Whilst a negative relationship between U and SI was expected on an energetic basis, it was unexpected that V_{grad} would also be negatively related to SI given that the feeding behaviour of juvenile salmonids makes them better suited to focal positions with low velocity that are situated close to zones of high velocity (Hayes & Jowett 1994; Booker et al. 2004). One explanation for this could be that the fish were not active due to low light levels. Fraser and Metcalfe (1997) found that juvenile Atlantic salmon were relatively inactive at illumination levels lower than those equivalent to dawn and dusk. However, observations of high nocturnal activity in summer (Gries et al. 1997) and lower rates of nocturnal hiding at temperatures above 9 °C (Valdimarsson et al. 1997) suggest that this species and life-stage will seek habitats suitable for feeding in darkness at the temperatures tested in this study, although we cannot rule out the possibility that fish were not searching for feeding stations because they were not fed during trials. Another possibility is that velocity gradients in the test section were not great enough to elicit a response from the fish. Mean velocity in gravel-bed rivers can range from near zero to >50 cm s^{-1} over small multiples of fish body length

(Roy et al. 2004; Buffin-Bélanger et al. 2006). The mean velocity range of $0<U<20$ cm s^{-1} within our test section is typical of the smallest range expected in natural settings (Buffin-Bélanger et al. 2006).

Negative values of τ_{uv} were associated with suitable habitat, whereas high positive values were not. This suggests that the fish exhibited a preference for locations at which there was a net flux of turbulent momentum towards the bed, presumably because this aided station-holding. Areas of high $|\tau_{uw}|$ were not preferentially occupied by the fish. The likely reason that Reynolds stresses were not included in the optimum count (*SI*) model is that maximal values were two orders of magnitude lower than reported in some previous laboratory experiments showing clear avoidance of high Reynolds stress zones (Silva et al. 2011; 2012). However, other studies found that similar Reynolds stresses to observed here elicited responses in terms of avoidance (Hockley et al. 2014) and swimming speed (Alexandre et al. 2013).

Locations downstream of hemispheres suitable for entraining ($<c_D$ downstream of hemisphere, where c_D is hemisphere diameter) and Kármán gaiting ($3<c_D<5$ downstream; Liao 2006) had relatively high *SI*. It remains uncertain whether the chaotic flow in the test section, with velocity spectra lacking pronounced peaks and relatively high Reynolds numbers compared with previous work (Enders et al. 2003; Liao et al. 2003, Liao 2006; Taguchi & Liao 2011), would be suitable for Kármán gaiting. It is also difficult to evaluate role of eddy length relative to body length (*bl*) as L_u was highly correlated with *U*. Relative eddy lengths in the test section included the range $0.6< L_u/bl<0.66$ thought to cause instability in cyprinid fish (Pavlov et al. 2000; Lupandin 2005; Tritico & Cotel 2010), but these values were associated with regions of high *SI*. It is possible that the flow was too chaotic (Enders &

Boisclair 2016) or eddy momentum was too low (Tritico & Cotel 2010) to elicit an avoidance response. Alternatively, juvenile Atlantic salmon may not be susceptible to such instabilities.

There are several factors that could have confounded our quantification of habitat selection in relation to the turbulent flow. Firstly, the fish were assumed to be responding to hydraulics but, although trials were performed in darkness and the artificial habitat features (hemispheres) were transparent, the possibility that fish used their lateral line system to select locations based on proximity to physical structures (*e.g.,* hemispheres or netting) cannot be ruled out. Secondly, the data analysis methods used ignored the possibility of strong spatial intercorrelation in the response of individual fish. If it is assumed, as the results suggest, that the fish chose energetically favourable locations then a third related factor is the possibility that they chose local, rather than global, energetic minima (*i.e.,* that they are only selecting the 'best' habitat from a small area). The use of random starting co-ordinates and the time allowed for acclimation and habitat exploration was an attempt to mitigate this. Furthermore, many fish were observed to be rapidly moving from one side or end of the test arena to the other, indicating that they were able to 'sample' the available habitat.

Implications for research and management

By integrating hydrodynamics and bioenergetics this work integrates two parallel trends in river research and management (Nikora 2010; Jørgensen et al. 2016). Bioenergetics models have been suggested as an advance on the simplistic, empirical approach taken by traditional hydraulic habitat models such as PHABSIM, yet their application has been limited because of their complexity and resource-intensiveness (Dunbar et al. 2012). The application of reliable habitat models is critical to evaluating the impacts of river barriers (Urabe et al. 2014), low flows (Rosenfeld & Ptolemy 2012), habitat degradation (Hafs et al. 2014), and stream

restoration (Railsback et al. 2013), all of which an involve modifications of the turbulent flow.

Our findings show how the hydraulic component of habitat models may be improved. We recommend the SC model of Enders et al. (2005) for inclusion as a parameter as it is a compromise between parsimony and causality, although we realise that many habitat modelling applications will lack the resources to collect sufficiently detailed data on the turbulent flow. Future research should investigate the accuracy of predictions made using this model in field settings that are likely to include a wider range of hydraulic conditions than studied here. A similar approach could be applicable to other species but relationships between flow and SC are likely to be species-specific. Turbulence may also be implicated in the energetic intake component of forage-based models for drift-feeding fish, in terms of the spatiotemporal variability in prey concentration and capture rates (Piccolo et al. 2014). This also warrants future research.

Conclusions

A recent accumulation of evidence has confirmed strong and complex relationships between turbulent flow and fish swimming energetics (*e.g.,* Enders et al. 2005; Tritico & Cotel 2010; Taguchi & Liao 2011; Lacey et al. 2012; Enders & Boisclair 2016) but these relationships have not yet been incorporated into models that predict position choice and habitat quality for fish. We establish, for the first time, a link between turbulent flow, swimming costs, and habitat selection in juvenile Atlantic salmon. The resulting habitat suitability curve based on the energetic costs of swimming in turbulent flow is in a format that can readily be implemented in habitat models.

Acknowledgements

This work was undertaken as part of a PhD studentship funded by the University of Worcester. Thanks to Bill Beaumont, Anton Ibbotson, Luke Scott, and Rasmus Lauridsen of the Game and Wildlife Conservation Trust and Bill Riley of CEFAS for fieldwork support, to Joe Booty for laboratory assistance, Paul Kemp, Jim Kerr, Laurence Lewis-Jones, and others from the International Centre for Ecohydraulics Research for assistance with planning and resources, and Ramsay Lind of Nortek UK for providing a Nortek Vectrino II ADV. Ana T. Silva was financed by the SafePass project (no. 244022) funded by the Research Council of Norway (RCN) under the ENERGIX program.

References

Alexandre CM, Quintella BR, Silva AT, Mateus CS, Romão F, Branco P, Ferreira MT, Almeida PR. 2013. Use of electromyogram telemetry to assess the behavior of the Iberian barbel (*Luciobarbus bocagei* Steindachner, 1864) in a pool-type fishway. Ecol. Eng. 51:191-202.

Boisclair C, Tang M. 1993. Empirical analysis of the influence of swimming pattern on the net energetic cost of swimming in fishes. J. Fish Biol. 42:169-183.

Booker DJ, Dunbar MJ, Ibbotson A. 2004. Predicting juvenile salmonid drift-feeding habitat quality using a three-dimensional hydraulic-bioenergetic model. Ecol. Model. 177:157-177.

Buffin-Bélanger T, Roy AG. 1998. Effects of a pebble cluster on the turbulent structure of a depth-limited flow in a gravel-bed river. Geomorphology 25:249–267.

Buffin-Bélanger T, Roy AG. 2005. 1 min in the life of a river: selecting the optimal record length for the measurement of turbulence in fluvial boundary layers. Geomorphology 68:77–94.

Buffin-Bélanger T, Rice S, Reid I, Lancaster J. 2006. Spatial heterogeneity of near-bed hydraulics above a patch of river gravel. Water Resour. Res. 42. DOI: 10.1029/2005WR004070.

Clifford NJ, French JR. 1993. Turbulence: Perspectives on flow and sediment transport. Chichester: Wiley. Chapter 1, Monitoring and modelling turbulent flow: Historical and contemporary perspectives; p. 1-34.

Cook CL, Coughlin DJ. 2010. Rainbow trout *Oncorhynchus mykiss* consume less energy when swimming near obstructions. J. Fish Biol. 77:1716–1723.

Dunbar MJ, Alfredsen K, Harby A. 2012. Hydraulic-habitat modelling for setting environmental flow needs for salmonids. Fish. Manag. Ecol. 19:500-517.

Enders EC, Boisclair D. 2016. Effects of environmental fluctuations on fish metabolism: Atlantic salmon *Salmo salar* as a case study. J. Fish Biol. 88:344-258.

Enders EC, Boisclair D, Roy AG. 2003. The effect of turbulence on the cost of swimming for juvenile Atlantic salmon (*Salmo salar*). Can. J. Fish. Aquat. Sci. 60:1149-1160.

Enders EC, Boisclair D, Roy AG. 2005. A model of total swimming costs in turbulent flow for juvenile Atlantic salmon (*Salmo salar*). Can. J. Fish. Aquat. Sci. 62:1079-1089.

ESRI. 2011. ArcGIS Desktop: Release 10. Redlands, California: Environmental Systems Research Institute.

Fausch KD. 1984. Profitable stream positions for salmonids: relating specific growth rate to net energy gain. Can. J. Zool. 62:441-451.

Fausch KD. 2014. A historical perspective on drift foraging models for stream salmonids. Environ. Biol. Fish. 97:453-464

Fraser NHC, Metcalfe NB. 1997. The costs of becoming nocturnal: feeding efficiency in relation to light intensity in juvenile Atlantic salmon. Funct. Ecol. 11:385-391.

Gries G, Whalen KG, Juanes F, Parrish DL. 1997. Nocturnal activity of juvenile Atlantic salmon (*Salmo salar*) in late summer: evidence of diel activity partitioning. Can. J. Fish. Aquat. Sci. 54:1408-1413.

Hafs AW, Harrison LR, Utz RM, Dunne T. 2014. Quantifying the role of woody debris in providing bioenergetically favouable habitat for juvenile salmon. Ecol. Model. 285:30-38.

Hayes JW, Jowett IG. 1994. Microhabitat models of large drift-feeding brown trout in three New Zealand Rivers. N. Am. J. Fish. Manage. 14:710-725.

Hayes JW, Goodwin E, Shearer KA, Hay J, Kelly L. 2016. Can Weighted Useable Area Predict Flow Requirements of Drift-Feeding Salmonids? Comparison with a Net Rate of Energy Intake Model Incorporating Drift–Flow Processes. Trans. Am. Fish. Soc. 145:589-609.

Heath AG. 1995. Water Pollution and Fish Physiology. CRC Press, Boca Raton.

Heggenes J. 1990. Habitat utilisation and preferences in juvenile Atlantic salmon (*Salmo salar*) in streams. Regul. River. 5:341–354.

Heggenes J, Saltveit SJ. 1990. Seasonal and spatial microhabitat selection and segregation in young Atlantic salmon, *Salmo salar* L., and brown trout, *Salmo trutta* L., in a Norwegian river. J. Fish Biol. 36:707-720.

Hill J, Grossman GD. 1993. An energetic model of microhabitat use for rainbow trout and rosyside dace. Ecology. 74:685-698.

Hockley FA, Wilson CAME, Brew A, Cable J. 2014. Fish responses to flow velocity and turbulence in relation to size, sex and parasite load. J. R. Soc. Interface. 11. DOI: 10.1098/rsif.2013.0814.

Hughes NF, Dill LM. 1990. Position choice by drift-feeding salmonids: model and test for arctic grayling (*Thymallus arcticus*) in subarctic mountain streams, Interior Alaska. Can. J. Fish. Aquat. Sci. 47: 2039-2048.

Jørgensen C, Enberg K, Mangel M. 2016. Modelling and interpreting fish bioenergetics: a role for behaviour, life-history traits and survival trade-offs. J. Fish Biol. 88:389-402.

Kennedy GJA, Strange CD. 1982. The distribution of salmonids in upland streams in relation to depth and gradient. J. Fish Biol. 20:579–591.

Lacey RWJ, Legendre P, Roy AG. 2007. Spatial-scale partitioning of in situ turbulent flow data over a pebble cluster in a gravel-bed river. Water Resour. Res. 43:W03416.

Lacey RWJ, Neary VS, Liao JC, Enders EC, Tritico HM. 2012. The IPOS framework: linking fish swimming performance in altered flows from laboratory experiments to rivers. River Res. Appl. 28:429–443.

Lancaster J, Downes BJ. 2010. Linking the hydraulic world of individual organisms to ecological processes: putting ecology into ecohydraulics. River Res. Appl. 26:385-403.

Lawless M, Robert A. 2001. Three-dimensional flow structure around small-scale bedforms in a simulated gravel-bed environment. Earth Surf. Process. Landf. 26:507–522.

Liao JC. 2006. The role of lateral line and vision on body kinematics and hydrodynamics preference of rainbow trout in turbulent flow. J. Exp. Biol. 209:4077-4090.

Liao JC. 2007. A review of fish swimming mechanics and behaviour in altered flows. Phil. Trans. R. Soc. B. 362:1973-1993.

Liao JC, Beal DN, Lauder GV, Triantafyllou MS. 2003. Fish exploiting vortices decrease muscle activity. Science. 302:1566-1569.

Lupandin AI. 2005. Effect of flow turbulence on swimming speed of fish. Biol. Bull. 32:461-466.

Meineri E, Deville AS, Grémillet D, Gauthier-Clerc M, Béchet, A. 2015. Combining correlative and mechanistic habitat suitability models to improve ecological compensation. Biol. Rev. 90:314-329.

Morantz DL, Sweeney RK, Shirvell CS, Longard DA. 1987. Selection of microhabitat in summer by juvenile Atlantic salmon (*Salmo salar*). Can. J. Fish. Aquat. Sci. 44:120–129.

Milhous RT, Wegner DL, Waddle T. 1984. Users guide to the Physical Habitat Simulation System (PHABSIM), Instream Incremental Flow Information Paper 11. US Fish and Wildlife Service: FWS/OBS-81/13 (revised).

Nikora V. 2010. Hydrodynamics of aquatic ecosystems: an interface between ecology, biomechanics and environmental fluid mechanics. River Res. Appl. 26:367-384.

Oliver MA. 1990. Kriging: A method of interpolation for Geographical Information Systems. Int. J. Geogr. Inf. Sci. 4:313-332.

Parsheh M, Sotiropoulos F, Porté-Agel F. 2010 Estimation of power spectra of acoustic Doppler velocimetry data contaminated with intermittent spikes. J. Hydraul. Eng. 136:368–378.

Pavlov DS, Lupandin AI, Skorobogatov MA. 2000. The effects of flow turbulence on the behaviour and distribution of fish. J. Icthyol. 40:232-S261.

Piccolo JJ, Frank BM, Hayes JW. 2014. Food and space revisited: The role of drift-feeding theory in predicting the distribution, growth, and abundance of stream salmonids. Environ. Biol. Fishes. 97:475-488.

Przybilla A, Kunze S, Rudert A, Bleckmann H, Brücker C. 2010. Entraining in trout: a behavioural and hydrodynamic analysis. J. Exp. Biol. 213, 2976–2986.

R Core Team. 2015. R: A language and environment for statistical computing. Vienna, Austria: R Foundation for Statistical Computing. ISBN 3-900051-07-0, URL http://www.R-project.org/.

Railsback SF, Gard M, Harvey BC, White JL, Zimmerman JK. 2013. Contrast of degraded and restored stream habitat using an individual-based salmon model. N. Am. J. Fish. Manage. 33:384-99.

Riehle MD, Griffith JS. 1993. Changes in habitat use and feeding chronology of juvenile rainbow trout (*Oncorhynchus mykiss*) in fall and the onset of winter in Silver Creek, Idaho. Can. J. Fish. Aquat. Sci. 50:2119-2128.

Rosenfeld JS, Ptolemy R. 2012. Modelling available habitat versus available energy flux: do PHABSIM applications that neglect prey abundance underestimate optimal flows for juvenile salmonids? Can. J. Fish. Aquat. Sci. 69:1920-34.

Roy AG, Buffin-Bélanger T, Lamarre H, Kirkbride AD. 2004. Size, shape and dynamics of large-scale turbulent flow structures in a gravel-bed river. J. Fluid Mech. 500:1-27.

Roy ML, Roy AG, Legendre P. 2010. The relations between 'standard' fluvial habitat variables and turbulent flow at multiple scales in morphological units of a gravel-bed river. River Res. Appl. 26:439-455.

Silva AT, Santos JM, Ferreira MT, Pinheiro AN, Katopodis C. 2011. Effects of water velocity and turbulence on the behaviour of Iberian barbel (*Luciobarbus bocagei*, Steindachner 1864) in an experimental pool-type fishway. River Res. Appl. 27:360–373.

Silva AT, Katopodis C, Santos JM, Ferreira MT, Pinheiro AN. 2012. Cyprinid swimming behaviour in response to turbulent flow. Ecol. Eng. 44:314-328.

Smith DL, Brannon EL. 2007. Influence of cover on mean column hydraulic characteristics in small pool riffle morphology streams. River Res. Appl. 23:125-139.

Symons PEK, Heland M. 1978. Stream habitats and behavioural interactions of underyearling and yearling Atlantic salmon (*Salmo salar*). J. Fish. Res. Board Can. 35, 175–183.

Taguchi M, Liao JC. 2011. Rainbow trout consume less oxygen in turbulence: the energetics of swimming behaviors at different speeds. J. Exp. Biol. 214:428–1436.

Tritico HM, Cotel AJ. 2010 The effects of turbulent eddies on the stability and critical swimming speed of creek chub (*Semotilus atromaculatus*). J. Exp. Biol. 213:2284-2293.

471 Urabe H, Nakajima M, Torao M, Aoyama T. 2014. Application of a bioenergetics model to
472 estimate the influence of habitat degradation by check dams and potential recovery of masu
473 salmon populations. Environ. Biol. Fishes. 97:587-598.

474 Valdimarsson SK, Metcalfe NB, Thorpe JE, Huntingford FA. 1997. Seasonal changes in sheltering:
475 effect of light and temperature on diel activity in juvenile salmon. Anim. Behav. 54:1405-1412.

476 Webb PW. 2004. Response latencies to postural differences in three species of teleostean fishes.
477 J. Exp. Biol. 207:955-961.

478 Wilkes MA, Maddock I, Visser F, Acreman M. 2013. Ecohydraulics: An integrated approach.
479 Chichester:Wiley. Chapter 1, Incorporating hydrodynamics into ecohydraulics: The role of
480 turbulence in the swimming and habitat selection of river-dwelling salmonids; p. 9-30.

481 Zuur AF, Ieno EN, Walker NJ, Saveliev AA, Smith GM. 2009. Mixed effects models and extensions
482 in ecology with R. New York: Springer.

Table 1 – Summary of predicted swimming costs for each fish, including the mean predicted SC expected at random ('Null'), and the probability (p) that each fish chose cells at random.

Fish	Mean SC_{pred} (mg O_2 h^{-1})	Behaviour	p
(Null)	0.5	NA	NA
1	0.08	Station-holding	0
2	0.19	Searching	0
3	0.48	Searching	0.37
4	0.29	Searching	0
5	0.03	Searching	0
6	0.23	Searching	0
7	0.09	Station-holding	0
8	0.03	Searching	0
9	0.64	Searching	0.99
10	0.71	Searching	0.99
11	0.02	Searching	0
12	0.14	Searching	0
13	0.03	Searching	0
14	0.05	Searching	0
15	0.32	Searching	0
16	0.1	Searching	0
17	0.28	Searching	0
18	0.002	Station-holding	0
19	0.58	Searching	0.95
20	0.03	Station-holding	0
21	0.02	Station-holding	0
22	0.39	Searching	0.008
23	0.039	Searching	0
24	0.05	Searching	0
25	0.06	Searching	0
26	0.33	Searching	0
27	0.33	Searching	0
29	0.41	Station-holding	0.04
30	0.11	Searching	0
31	0.46	Searching	0.24
32	1.38	Searching	1
33	0.3	Searching	0
35	0.02	Station-holding	0
36	0.36	Station-holding	0.0006
37	0.06	Station-holding	0
38	0.21	Station-holding	0
39	0.03	Station-holding	0
41	0.01	Station-holding	0
43	0.05	Station-holding	0
44	0.25	Station-holding	0
45	0.13	Station-holding	0
46	0.29	Station-holding	0

Table 2 – Results of ZINB modelling for the swimming costs model.

Term	Estimate	SE	z value	*p*
	$g(\mu)$			
(Intercept)	0.1009	0.1521	0.664	0.507
CR	-0.8979	0.1129	-7949	< 0.001
log (theta)	-3.1132	0.1287	-24.186	< 0.001
	$g(\pi)$			
(Intercept)	-1.829	1.127	-1.622	0.105
CR	-1.214	0.817	-1.486	0.137
			Log-lik = -3504 on 5 df	
			AIC = 6967.16	

Table 3 – Summary of ZINB model selection for the bespoke hydrodynamic habitat model.

Dropped term	df	AIC	LR test
None	11	6926.53	
U from count model	10	6938.33	$X^2 = 13.8$ ($df = 1$, $p = 2.03 \times 10^{-9}$)
V_{grad} from count model	10	6932.62	$X^2 = 8.0965$ ($df = 1$, $p = 0.00444$)
τ_{uv} from count model	10	6925.05	$X2 = 0.5291$ ($df = 1$, $p = 0.467$)
Iτ_{uw}I from count model	10	6927.45	$X^2 = 2.92$ ($df = 1$, $p = 0.0875$)
U from binomial model	10	6936.66	$X^2 = 12.128$ ($df = 1$, $p = 4.97 \times 10^{-4}$)
V_{grad} from binomial model	10	6938.52	$X^2 = 13.989$ ($df = 1$, $p = 1.84 \times 10^{-4}$)
τ_{uv} from binomial model	10	6945.09	$X^2 = 20.567$ ($df = 1$, $p = 5.76 \times 10^{-7}$)
Iτ_{uw}Ifrom binomial model	10	6964.76	$X^2 = 40.231$ ($df = 1$, $p = 2.26 \times 10^{-10}$)
τ_{uv} and Iτ_{uw}I from count model	9	6925.55	$X^2 = 3.0203$ ($df = 2$, $p = 0.221$)
τ_{uv} and Iτ_{uw}Ifrom binomial model	9	6964.11	$X^2 = 41.584$ ($df = 2$, $p = 9.34 \times 10^{-10}$)
τ_{uv} and Iτ_{uw}I from both models	7	6963.14	$X^2 = 44.614$ ($df = 4$, $p = 4.78 \times 10^{-9}$)

489 Table 4 – Results of ZINB modelling for the optimal bespoke hydrodynamic model.

Term	Estimate	SE	z value	*p*
	$g(\mu)$			
(Intercept)	1.31874	0.18825	7.005	2.47×10^{-12}
U	-0.14748	0.02827	-5.217	1.82×10^{-7}
V_{grad}	-0.29105	0.09463	-3.076	0.0021
log (theta)	-2.62764	0.099	-26.543	$< 2 \times 10^{-16}$
	$g(\pi)$			
(Intercept)	0.47686	0.27764	1.718	0.08588
U	0.16404	0.05232	3.135	0.00172
V_{grad}	-0.60384	0.17324	-3.485	4.91×10^{-4}
τ_{uv}	-0.05798	0.01423	-4.074	4.62×10^{-5}
Iτ_{uv}I	-0.09924	0.03010	-3.297	9.77×10^{-4}
			Log-lik = -3454 on 9 df	
			AIC = 6925.55	

490

491

Figure 1 – Map of test section and sample locations for acoustic Doppler velocimeter (ADV) measurements.

Figure 2 – Maps of (a) mean velocity, (b) turbulence intensity, (c) average eddy length, (d, e) Reynolds shear stresses, and (f) resultant velocity vectors illustrating the sampling locations in the test area of the experimental stream channel.

Figure 3 – Example velocity spectra over a large hemisphere (a-d) and a small (e-h) hemispheres located at x=125, z =185, and x=135, z=17.5 respectively, where x and z are streamwise and spanwise coordinates within the test arena (cm). Spectra shown for locations upstream (z-5 cm) and downstream (*e.g.*, z+5 cm) of hemispheres.

Figure 4 – Map of predicted swimming costs.

Figure 5 – Maps illustrating (a) typical station-holding (fish 9) and searching (fish 38) behaviours and (b) the habitat selection index, a measure of cell occupancy by n=46 fish with t=121 observations per fish (see equation 6).

Figure 6 – Null distribution of predicted swimming costs based on 10,000 bootstrap samples of 121 random cells from the artificial habitat.

Figure 7 – (a) Count (selection index, *SI*) and (b) binomial (probability of false zero, *p*) results for the predicted swimming costs (SC_{pred}) model. Count model predictions standardised (μ_i / μ_{max}) to visualise results. Symbols denote observed *SI* for each cell.

Figure 8 – (a-b) Count (selection index, *SI*) and (c-f) binomial (probability of false zero, *p*) results for the optimal bespoke hydrodynamic habitat model, including parameters mean resultant velocity (*U*), spatial velocity gradient (V_{grad}) and Reynolds stresses in the streamwise vertical (τ_{uv}) and horizontal (τ_{uw}, absolute) planes. Count model results standardised (μ_i / μ_{max}) and all model predictions smoothed using a loess smoother (span = 0.5) to visualise results. Symbols denote observed *SI* for each cell.

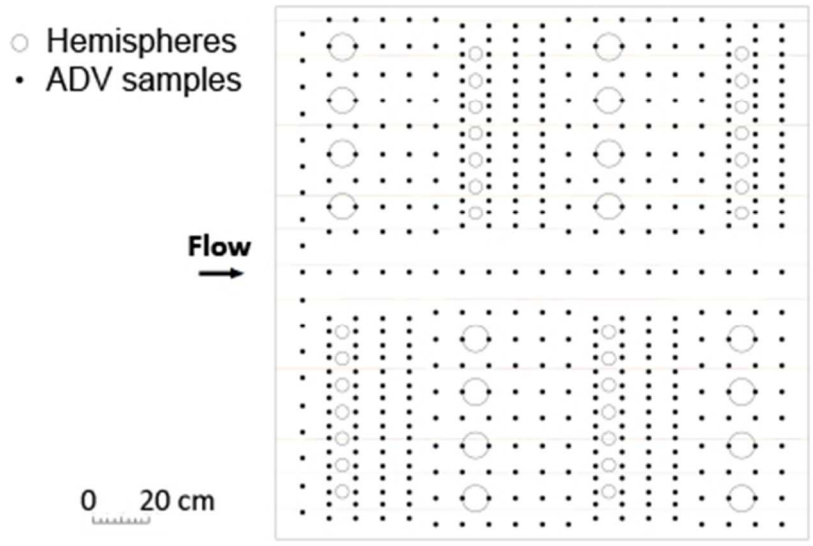

Figure 1 – Map of test section and sample locations for acoustic Doppler velocimeter (ADV) measurements.
[Figure 1 near here]
144x98mm (72 x 72 DPI)

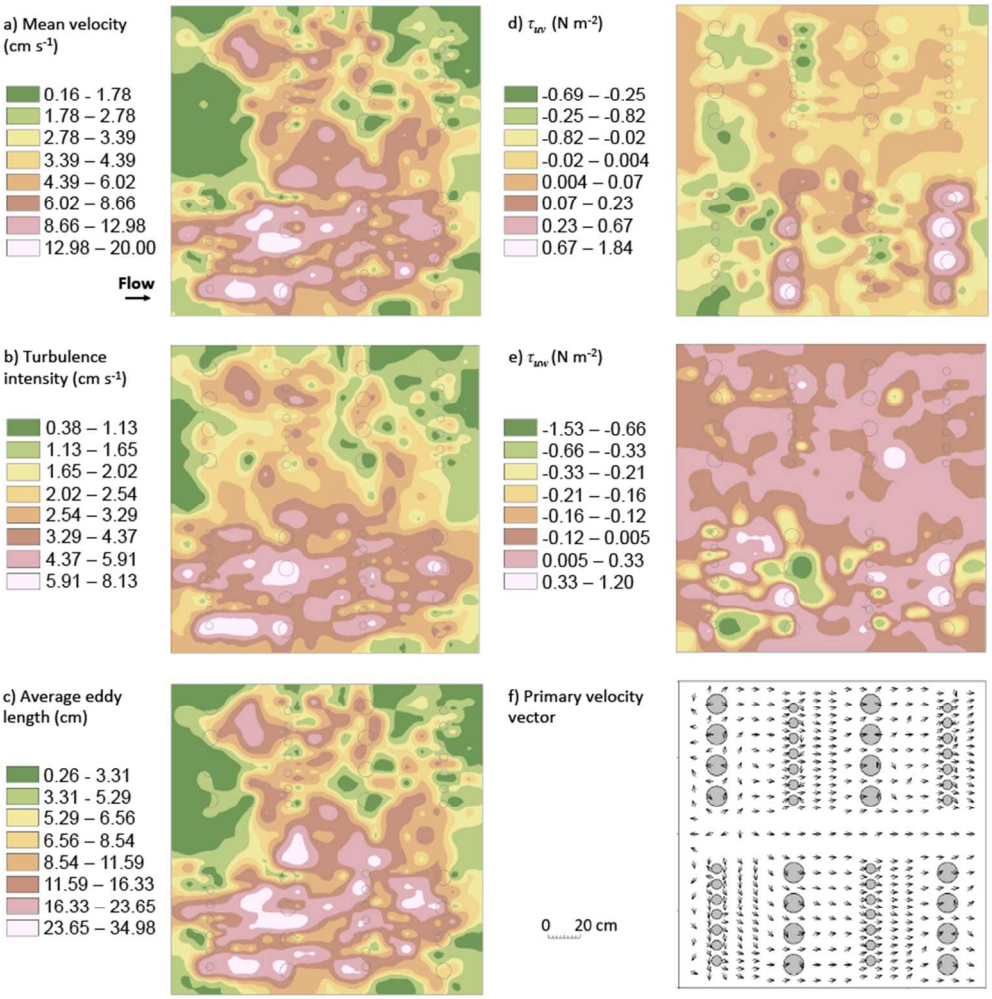

Figure 2 – Maps of (a) mean velocity, (b) turbulence intensity, (c) average eddy length, (d, e) Reynolds shear stresses, and (f) resultant velocity vectors illustrating the sampling locations in the test area of the experimental stream channel.
[Figure 2 near here]
311x314mm (72 x 72 DPI)

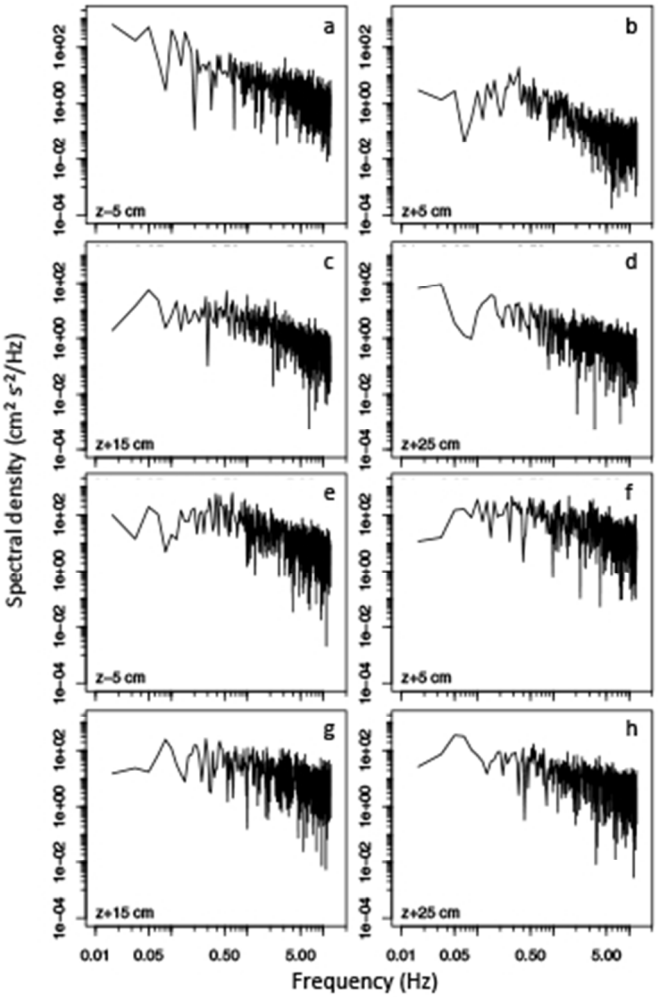

Figure 3 – Example velocity spectra over a large hemisphere (a-d) and a small (e-h) hemispheres located at x=125, z =185, and x=135, z=17.5 respectively, where x and z are streamwise and spanwise coordinates within the test arena (cm). Spectra shown for locations upstream (z-5 cm) and downstream (e.g., z+5 cm) of hemispheres.

[Figure 3 near here]

28x42mm (300 x 300 DPI)

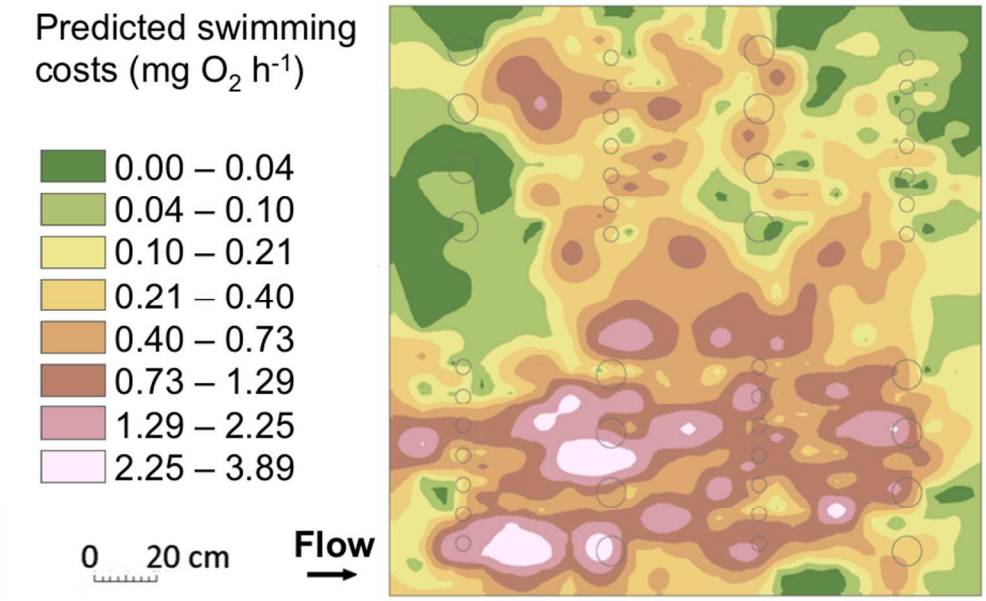

Figure 4 – Map of predicted swimming costs.
[Figure 4 near here]
158x98mm (150 x 150 DPI)

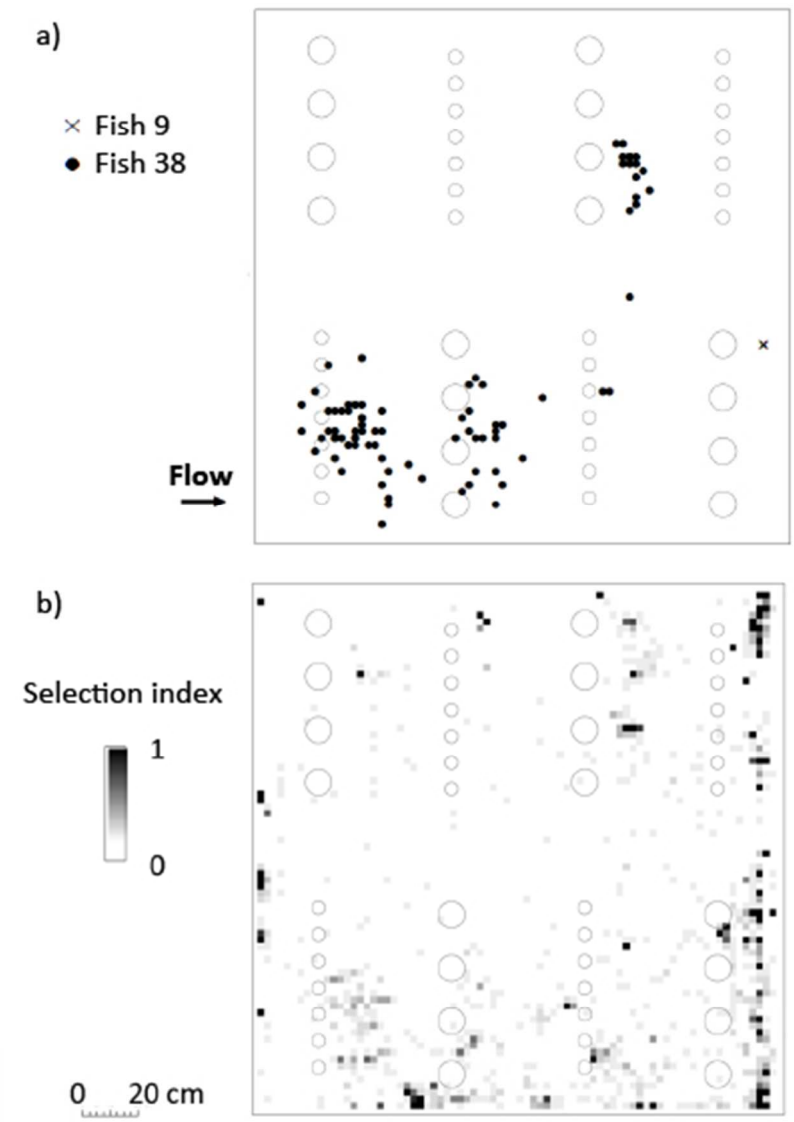

Figure 5 – Maps illustrating (a) typical station-holding (fish 9) and searching (fish 38) behaviours and (b) the habitat selection index, a measure of cell occupancy by n=46 fish with t=121 observations per fish (see equation 6).
[Figure 5 near here]
143x198mm (72 x 72 DPI)

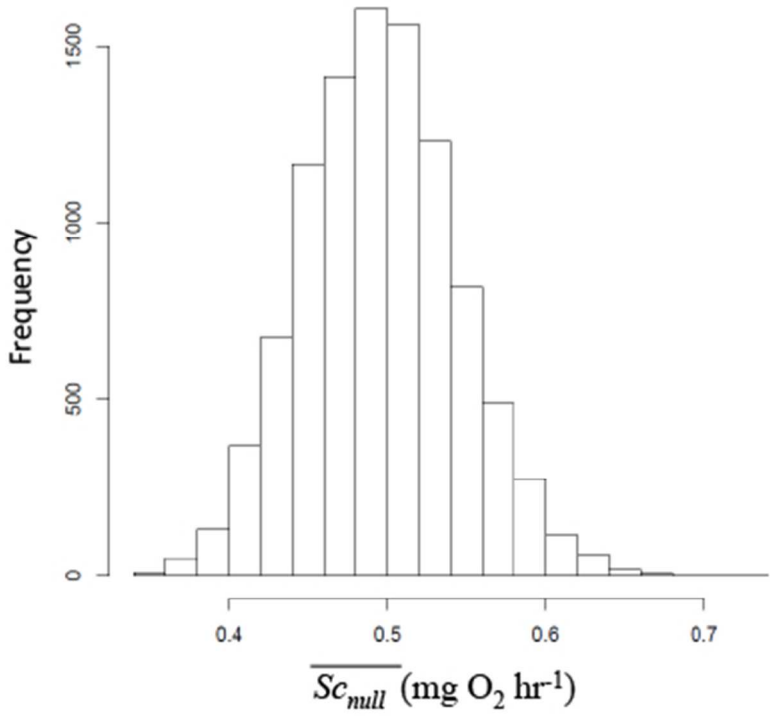

Figure 6 – Null distribution of predicted swimming costs based on 10,000 bootstrap samples of 121 random cells from the artificial habitat.
[Figure 6 near here]
141x127mm (72 x 72 DPI)

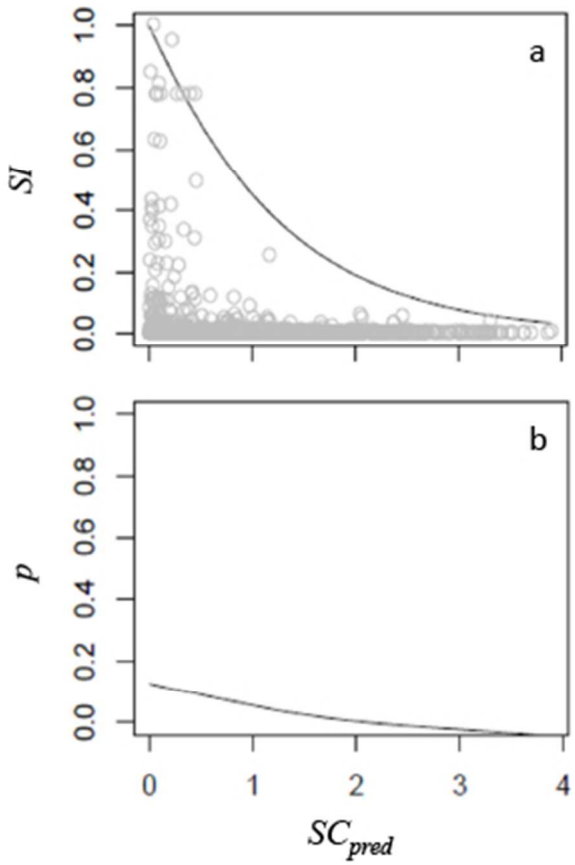

Figure 7 – (a) Count (selection index, SI) and (b) binomial (probability of false zero, p) results for the predicted swimming costs (SCpred) model. Count model predictions standardised (μi / μmax) to visualise results. Symbols denote observed SI for each cell.
[Figure 7 near here]
104x153mm (72 x 72 DPI)

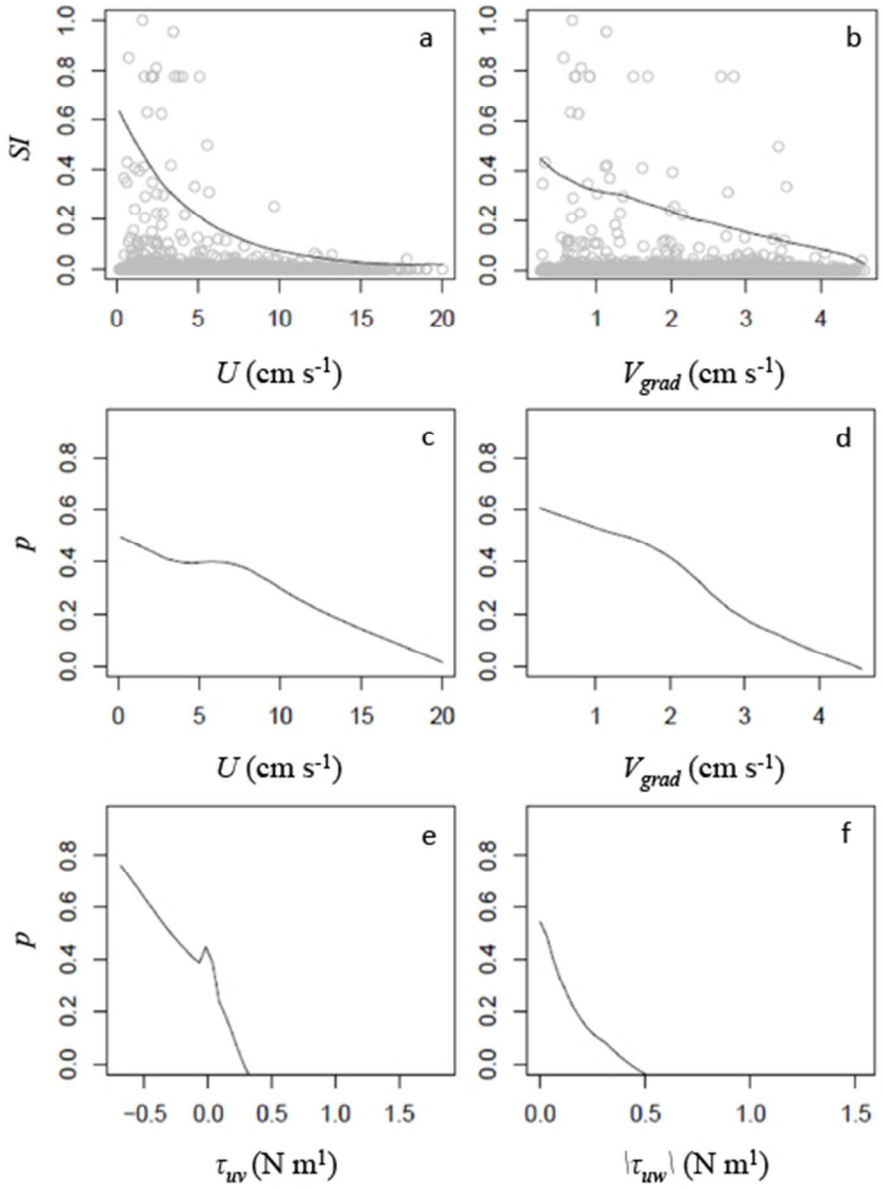

Figure 8 – (a-b) Count (selection index, SI) and (c-f) binomial (probability of false zero, p) results for the optimal bespoke hydrodynamic habitat model, including parameters mean resultant velocity (U), spatial velocity gradient (Vgrad) and Reynolds stresses in the streamwise vertical (τuv) and horizontal (τuw, absolute) planes. Count model results standardised (μi / μmax) and all model predictions smoothed using a loess smoother (span = 0.5) to visualise results. Symbols denote observed SI for each cell.
[Figure 8 near here]
183x242mm (72 x 72 DPI)